VCU VIRGINIA COMMONWEALTH UNIVERSITY

Virginia Commonwealth University
VCU Scholars Compass

Electrical and Computer Engineering Publications

Dept. of Electrical and Computer Engineering

2007

Epitaxial lateral overgrowth of a-plane GaN by metalorganic chemical vapor deposition

X. Ni
Virginia Commonwealth University, nix@vcu.edu

U. Ozgur
Virginia Commonwealth University, uozgur@vcu.edu

H. Morkoç
Virginia Commonwealth University, hmorkoc@vcu.edu

Z. Liliental-Weber
Lawrence Berkeley National Laboratory

H. O. Everitt
Duke University

Follow this and additional works at: http://scholarscompass.vcu.edu/egre_pubs

Part of the Electrical and Computer Engineering Commons

Epitaxial lateral overgrowth of *a*-plane GaN by metalorganic chemical vapor deposition

X. Ni,[a] Ü. Özgür, and H. Morkoç
Department of Electrical Engineering, Virginia Commonwealth University, Richmond, Virginia 23284, USA

Z. Liliental-Weber
Lawrence Berkeley National Laboratory 62/203, Berkeley, California 94720, USA

H. O. Everitt
Department of Physics, Duke University, Durham, North Carolina 27708, USA
and U.S. Army Aviation and Missile Research, Development and Engineering Center,
Redstone Arsenal, Alabama 35898, USA

We report on epitaxial lateral overgrowth (ELO) of $(11\bar{2}0)$ *a*-plane GaN by metalorganic chemical vapor deposition. Different growth rates of Ga- and N-polar wings together with wing tilt create a major obstacle for achieving a smooth, fully coalesced surface in ELO *a*-plane GaN. To address this issue a two-step growth method was employed to provide a large aspect ratio of height to width in the first growth step followed by enhanced lateral growth in the second by controlling the growth temperature. By this method, the average ratio of Ga- to N-polar wing growth rate has been reduced from 4–6 to 1.5–2, which consequently reduced the wing-tilt induced height difference between the two approaching wings at the coalescence front, thereby making their coalescence much easier. Transmission electron microscopy showed that the threading dislocation density in the wing regions was 1.0×10^8 cm^{-2}, more than two orders of magnitude lower than that in the window regions $(4.2 \times 10^{10}$ cm$^{-2})$. However, a relatively high density of basal stacking faults of 1.2×10^4 cm^{-1} was still present in the wing regions as compared to *c*-plane GaN, where they are rarely observed away from the substrate. Atomic force microscopy (AFM) measurements showed two orders of magnitude higher density of surface pits in the window than in the wing regions, which were considered to be terminated by dislocations (partial ones related to stacking faults and full ones) on the surface. The existence of basal stacking faults was also revealed by AFM measurements on the *a*-plane ELO sample after wet chemical etching in hot H_3PO_4/H_2SO_4 (1:1). The extensions of Ga-polar wings near the meeting fronts were almost free of stacking faults. The improvement of crystalline quality in the overgrown layer by ELO was also verified by near field scanning optical microscopy and time-resolved photoluminescence measurements; the former showing strongly enhanced luminescence from the wing regions, and the latter indicating longer decay times (0.25 ns) compared to a standard *a*-plane GaN template (40 ps). © *2007 American Institute of Physics.*
[DOI: 10.1063/1.2773692]

I. INTRODUCTION

The strong electric field produced by spontaneous and strain-induced piezoelectric polarizations in the *c*-axis-oriented hexagonal GaN system causes spatial separation of electrons and holes in quantum well active regions of optical devices.[1] Consequently, the radiative lifetime is increased[2] at the expense of the quantum efficiency[3] and a redshift occurs in the emission. Injection of carriers negates the extent of the resulting redshift. These problems can be overcome by growing *m*-plane or *a*-plane hexagonal GaN, which are nonpolar. Of these two common nonpolar planes of GaN, the *a*-plane GaN can be grown on *r*-plane sapphire using molecular beam epitaxy,[4] or metalorganic chemical vapor deposition (MOCVD).[5,6] Recent studies on *a*-plane AlGaN/GaN quantum wells[7,8] and related light emitting diodes[9] have already demonstrated the absence of a polarization-induced electric field. In order to realize high-performance nitride devices, the epitaxial lateral overgrowth (ELO) method[10] has been used to reduce the density of threading dislocations in *a*-plane GaN using MOCVD.[11,12] However, one must consider the wing tilt, which has been shown to be an important factor also for *c*-plane GaN ELO.[13] In this article, we investigate the effects of MOCVD growth parameters on the overgrown *a*-plane GaN material quality inclusive of the wing tilt, structural, and optical properties.

II. EXPERIMENT

The $(11\bar{2}0)$ *a*-plane GaN films investigated in this study were grown on $(1\bar{1}02)$ *r*-plane sapphire substrates.[6] For the ELO, 1.5 μm thick *a*-plane GaN templates with low-temperature grown GaN nucleation layers were used. A SiO$_2$ layer approximately 100 nm thick was grown on the *a*-plane GaN template by remote plasma enhanced chemical vapor deposition. A striped mask pattern was transferred onto

[a] Electronic mail: nix@vcu.edu

SiO$_2$/GaN/sapphire using conventional photolithography and buffered oxide etch. The pattern consisted of 4 μm wide open windows and 10 or 20 μm wide SiO$_2$ stripes that were oriented along the (1$\bar{1}$00) direction (i.e., the *m* axis) of GaN that would cause the lateral growth fronts to advance along the *c$^+$* and *c$^-$* directions. The patterned template was then reloaded into the MOCVD chamber for overgrowth. Three *a*-GaN ELO samples were investigated for this particular study, samples A, B, and C. Samples A and B were grown with trimethylgallium and NH$_3$ flow rates of 157 μmol/min and 3000 sccm, respectively. Sample A was grown in a single step at 1050 °C for 3 h while sample B was grown in two stages: at 1000 °C for 2 h in stage I and at 1050 °C for 3 h in stage II. Sample C was grown using 560 sccm NH$_3$ in the second stage with the rest of the conditions kept identical to those employed for sample B. All three samples were grown on two separate templates containing 10 and 20 μm wide SiO$_2$ stripes placed side by side in the growth chamber.

The as-grown samples were characterized by scanning electron microscopy (SEM), high-resolution x-ray diffraction (XRD), transmission electron microscopy (TEM), atomic force microscopy (AFM), photoluminescence (PL), time-resolved PL (TRPL), and near field scanning optical microscopy (NSOM). Low-temperature PL was performed on GaN layers using 325 nm excitation from a HeCd laser. TRPL measurements were performed at room temperature using 325 nm excitation from a Ti:sapphire oscillator/regenerative amplifier pumped optical parametric amplifier and a Hamamatsu streak camera. The excitation density was kept well below the stimulated emission threshold and the spot size ($\sim$350 μm diameter) was much larger compared to the wing/window widths. NSOM measurements were performed at room temperature in the illumination mode where a 325 nm HeCd laser was used for excitation through a metal-coated cantilevered optical fiber probe with a 350 nm aperture. NSOM PL intensity mapping was carried out using a photomultiplier tube to collect the overall PL spectrum with the scattered and reflected laser light blocked with an optical filter. The cross-sectional SEM measurements were performed on the 20 μm stripe samples for a better view of the overgrown layer dimensions. The rest of the analysis was focused on the 10 μm stripe samples unless otherwise indicated.

III. RESULTS AND DISCUSSION

The plan-view SEM image of sample A in Fig. 1(a) shows that the *a*-plane GaN stripes have vertical (0001) and (000$\bar{1}$) sidewalls after 0.5 h of overgrowth with no other facets present. As shown in Fig. 1(c) the surface of sample A was fully coalesced after a total of 3 h of overgrowth but with striations along and steps perpendicular to the *c* axis. The cross-sectional SEM image [Fig. 1(b)] clearly shows that the wings with Ga polarity are 4–6 times wider than those with N polarity. As a consequence of the inherent wing tilt and significantly different growth rates of the two opposing wings, a clear height difference appears at the coalescence front, as illustrated by the schematics in Figs. 2(a) and 2(b). This wing-tilt-induced height difference causes a sig-
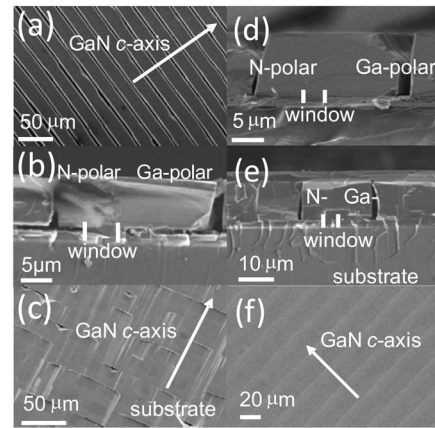

FIG. 1. Plan-view SEM images for sample A after (a) 0.5 and (c) 3.0 h of growth. (b) Cross-sectional SEM image for sample A after 3 h of growth. (d) Cross-sectional SEM image for sample B after 2 h of growth at 1000 °C. (e) Cross-sectional and (f) plan-view SEM images for sample B after a total of 5 h of growth.

nificant surface undulation in addition to defects at the coalescence fronts of *a*-plane GaN and is the origin of the steps observed in Fig. 1(c). However, the height difference is mainly a consequence of the difference in growth rates of the Ga- and N-polar wings. In order to obtain uniform coalescence and smooth surface, this height difference should be decreased or even eliminated if possible by reducing the difference between the widths or growth rates of the two opposing wings.

Our experimental results suggest that the growth temperature is a highly effective parameter to control the difference in the growth rates of the Ga- and N-polar wings. Therefore, for sample B, a two-stage growth method was employed. A growth temperature of 1000 °C was used in stage I to favor vertical growth while maintaining a relatively
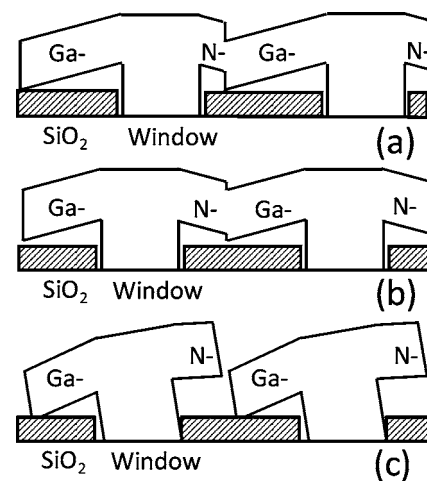

FIG. 2. Schematics for *a*-plane GaN ELO showing the origin of the height difference between two neighboring wings (not in exact proportion), with Ga- to N-polar wing width ratios of (a) 5:1 and (b) 1.6:1. The larger this ratio, the larger the height difference is between the two opposite wings at the coalescence fronts. (c) Schematic showing the inclination of the growth planes due to the 1.05° miscut of the *r*-plane sapphire toward its [0001] *c* axis. The miscut of the substrate, and therefore, the resultant inclination of the GaN growth planes is the origin of the elevated meeting fronts observed from AFM.
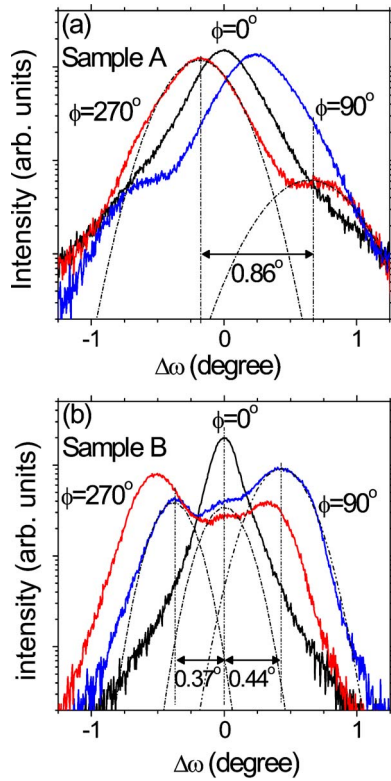
FIG. 3. (Color online) XRD rocking curve data for (a) sample A and (b) sample B with different ϕ angles. The dashed lines correspond to the multiple Gaussian fits to the rocking curve data.
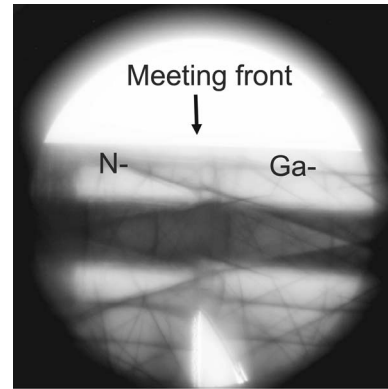

FIG. 4. ($\bar{2}110$) Kikuchi lines from large angle convergent beam electron diffraction at the meeting front of the two opposing wings for sample A. Note that the Kikuchi lines are shifted across the meeting front.

low lateral growth rate which is not drastically different for the lateral Ga- and N-polar fronts at this temperature. Figure 1(d) shows that, after the stage I growth, the sidewalls of *a*-GaN stripes are composed of facets other than (0001) or (000$\bar{1}$). It is noted that most of the lateral growth has been achieved with no coalescence during stage I where the Ga- to N-polar wing width ratio is close to 1.5–2. The growth temperature was elevated to 1050 °C in stage II to enhance the lateral growth for complete coalescence. A quite smooth surface was achieved after full coalescence, and the Ga-polar wing was only 1.5–2 times wider than the N-polar wing as shown in Figs. 1(e) and 1(f). These results indicate that the uneven growth rates of Ga- and N-polar wings could be suppressed to reduce the step height at the meeting fronts by enhancing the vertical growth rate during the early stages of the growth.

The wing tilt is an important issue inherent in conventional ELO. To determine the wing tilt angles of samples A and B, XRD rocking curve measurements were carried out with three different ϕ angles, where ϕ is the angle of rotation about the sample surface normal and is defined as 0° when the projection of incident x-ray beam is parallel to the SiO$_2$ mask stripes. As shown in Figs. 3(a) and 3(b), both samples exhibited only one *a*-plane GaN diffraction peak when ϕ = 0°, with a full width at half maximum (FWHM) of 0.40° and 0.19° for samples A and B, respectively. However, two and three peaks were observed for samples A and B, respectively, for ϕ = 90° (the projection of the incident x-ray beam is perpendicular to the mask stripes), with the peak order reversed for ϕ = 270°. The FWHM values for the strongest

peaks are 0.44° and 0.40° for samples A and B, respectively. The strongest peak observed for sample A is from the Ga-polar wings as determined from the XRD geometry used, since the surface area of the Ga-polar wing is much larger than that from the combination of the N-polar wing and the window as verified from the SEM images discussed earlier. Therefore, the weak peak is assumed to be from the windows and/or N-polar wings. The separation between the two peaks indicates a tilt angle of 0.86°, which is much larger than that obtained from the large angle convergent beam electron diffraction (LACBED) (0.25°) (see Fig. 4). This discrepancy may be attributed to the local nature of the LACBED measurement, while XRD characterizes a much larger area and provides a value averaged over a large area. As shown in Fig. 3(b), sample B exhibits smaller XRD linewidths compared to sample A, which indicates improved crystalline quality. Moreover, peaks from all three ELO regions are distinguishable for this sample. The strongest peak in Fig. 3(b) is from the Ga-polar wings (0.44° tilt), while the central one is from the crystal plane in the windows, and the third is from the N-polar wings (0.37° tilt).

TEM studies indicated a significant reduction in threading dislocation densities by ELO. For sample A, the threading dislocation density was reduced from 4.2×10^{10} cm^{-2} in the windows to 1.0×10^{8} cm^{-2} in the wings, as evidenced in Fig. 5(a). However, a relatively high density of basal stacking faults (BSFs), 1.2×10^{4} cm^{-1}, is still present in the wing areas compared to 1.3×10^{6} cm^{-1} in the windows, due to the low formation energy of stacking faults in the basal plane during *a*-plane GaN growth.[14,15] It is important to note that these stacking faults propagate to the *a*-plane sample surface, and may therefore intersect any active area of a device grown on such layers. In fact, the high density of BSFs in the windows results from the propagation of the BSFs generated in the *a*-plane GaN template freely into the windows, while they are blocked by the SiO$_2$ mask on the wing regions. The existence of BSFs in the wing regions could be partially due to the misalignment between the growth windows and the GaN *m* axis, as will be discussed later. Dislocations were also found at the meeting fronts of sample A, as in the case of *c*-plane ELO.[16] As evidenced in Fig. 5(b), sample B also displayed nearly two orders of magnitude reduction of dislo-
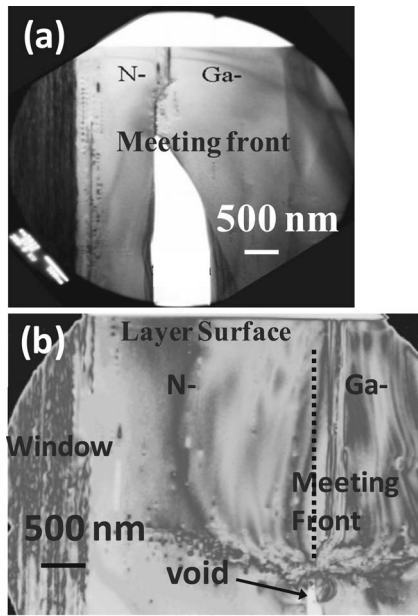
FIG. 5. Cross-sectional TEM images showing the window and wing regions for (a) sample A and (b) sample B.

FIG. 6. (Color online) (a) 30 μm$\times$30 μm AFM image for sample B. (b) 4 μm$\times$4 μm AFM image near the window and N-polar wing boundary of sample B, showing different surface pit densities for the window and the wing.

cations in the wings and generation of new dislocations at the meeting fronts. When the neighboring wings coalesce, a grain boundary is formed on the prismatic plane with the shift vector parallel to [0001]. These boundaries sometimes eliminate BSFs propagating from the substrate, but often are the sources of new defects propagating to the surface.

Tapping-mode AFM measurements were conducted to study the surface morphology of fully coalesced sample B. As shown in Fig. 6(a), the surface exhibits striated features along the c axis in both the window and the wing regions. Contrary to the c-plane GaN ELO, the meeting fronts are higher than the windows by about 60–100 nm. This is due to a 1.05° miscut of the r-plane sapphire toward its [0001] c-axis determined from XRD analysis. As illustrated in Fig. 2(c), this miscut results in the inclination of the GaN a-plane toward [0001] by 1.05°, which is larger than the wing tilt of ~0.4°, and an upward slope of the N-polar wings with respect to the substrate surface, giving rise to the elevation at the meeting fronts after coalescence. This inclination of the GaN a plane, which is congruent with the miscut of the r-plane sapphire substrate, has its origin in the dominance of the GaN growth along its c axis. This is the direction along which the lateral growth fronts in a-plane ELO advance. With increasing substrate miscut, the GaN a plane and the wings are still expected to follow the miscut angle. Growth on m-plane sapphire (that may be considered as 32.4° miscut of the r plane away from the c axis) has been shown to produce a-plane GaN surfaces inclined by 32.4° with respect to the substrate.[17] This important observation may pave the way for epitaxial growth of patterned GaN surfaces with well-defined crystal planes (both polar and nonpolar) on miscut sapphire substrates without the need for additional processing steps.

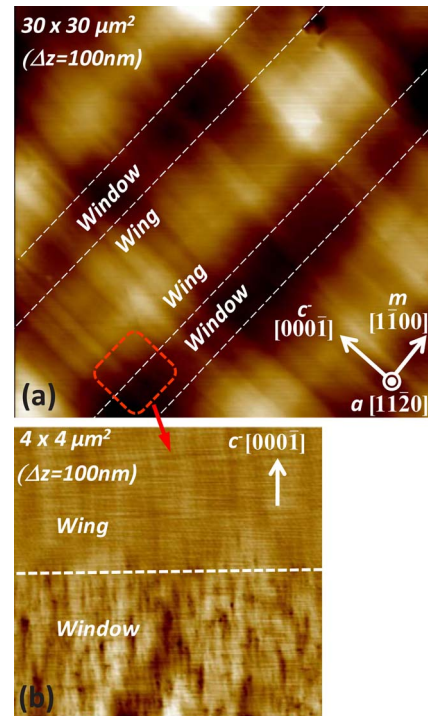AFM measurements on the as-grown a-plane GaN ELO samples revealed significantly different densities of surface pits in the window and wing regions, which are usually attributed to dislocation terminations at the surface.[5] Figure 6(b) shows an AFM image near the window and N-polar wing boundary for sample B, where the pit density in the windows ($\sim3.0\times10^9$ cm^{-2}) is approximately two orders of magnitude larger than that in the wings ($\sim3.7\times10^7$ cm^{-2}). The pit density deduced from AFM is smaller than the dislocation density obtained from TEM, most probably because pure edge dislocations are harder to observe in AFM, making the apparent total dislocation density smaller. However, both AFM and TEM results confirm the effective dislocation reduction in a plane by ELO. Additionally, an etch pit density study was also carried out to estimate the dislocation densities. As shown in Fig. 7(a), the pits in the windows were enlarged and became more obvious after etching in a mixed H$_3$PO$_4$/H$_2$SO$_4$ (1:1) solution for 20 min at 200 °C, and the pit densities were similar to those before etching. In the wing regions, the etching has generated clear but inhomogeneously distributed steps extending along the GaN m direction. In the N-polar wing regions, the steps were uniform and dense, while in the Ga-polar wing regions, most steps were observed near the windows, and the sectors near the meeting fronts were free of steps. The distribution of these steps is very similar to that of the stacking faults observed from cross-sectional TEM in Fig. 7(b). The density of these etching-formed steps is around 2×10^4 cm^{-1} in the Ga-polar wings and 6×10^4 cm^{-1} in the N-polar wings, respectively, giving an average density of $3-4\times10^4$ cm^{-1} in the wings. These values are in good agreement with those obtained from TEM. Currently, there is no report regarding wet etching of nonpolar GaN and the origin of these steps. Wet chemical etching has often been employed in the study of
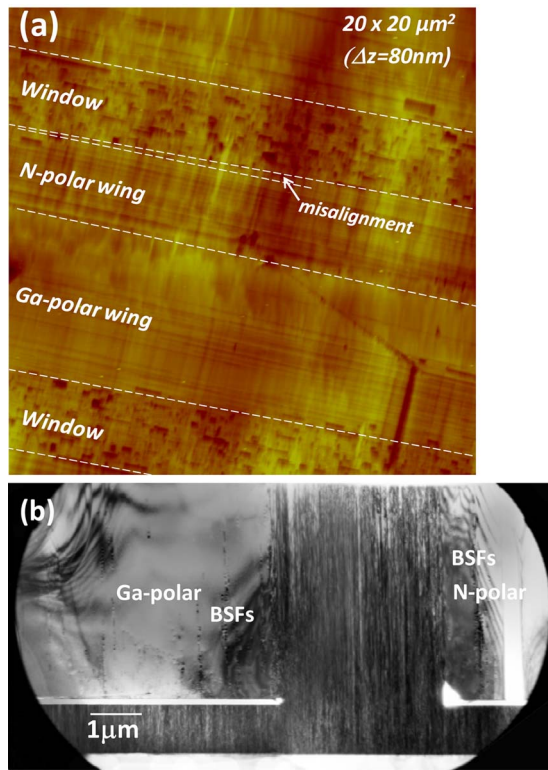
FIG. 7. (Color online) (a) 20 μm$\times$20 μm AFM image for sample B after etching in a mixed H_3PO_4/H_2SO_4 (1:1) solution for 20 min at 200 °C. (b) Cross-sectional TEM image for sample B showing the distributions of basal stacking faults in the wings, with most of them located near window regions.

FIG. 8. (Color online) (a) AFM and (b) NSOM scans from a 40 μm $\times$40 μm area of *a*-GaN ELO sample B. (c) AFM and (d) NSOM scans from a 75 μm$\times$75 μm area of *a*-GaN ELO sample C (20 μm-stripe sample). The vertical scale bars in (a) and (b) correspond to 85 and 150 nm, respectively.

bulk SiC growth to reveal stacking faults on cleavage planes, and basal stacking faults have been observed as linear steps on wet-etched prismatic planes of SiC.[18–20] Therefore, we suggest that the steps formed after etching of the *a*-GaN ELO samples might be due to the presence of basal stacking faults propagating to the surface. Therefore, wet etching offers a very convenient and effective means to characterize the structural defects, especially the stacking faults in nonpolar or semipolar GaN.

As shown in Fig. 7(a), there is a small misalignment (around 2°–4°) between the windows and the steps (oriented along the GaN *m* axis) formed after etching that represent the BSFs propagating to the surface. This indicates that the windows, i.e., the SiO$_2$ stripes are not perfectly aligned along the *m* axis of GaN, which may have led to the observation of BSFs in the wing areas near the windows. Extreme caution should be taken during the alignment of the SiO$_2$ mask for nonpolar ELO as BSFs could propagate from the template and through the windows into the wings if the windows are not oriented parallel to the GaN basal plane.[21]

In order to assess the improvement in optical quality with the two-step ELO, NSOM was carried out on samples B and C. Figures 8(a) and 8(b) show the AFM and NSOM images, respectively, taken from a 40 μm$\times$40 μm area of sample B. The window and wing regions, as well as the meeting fronts are clearly distinguishable from the NSOM image of Fig. 8(b). The windows appear as dark regions, and the narrow and the wide bright regions are due to N- and
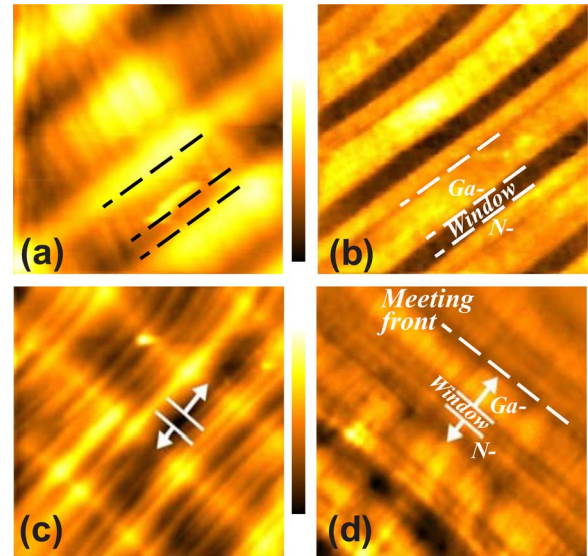
Ga-polar wings, respectively, with no significant difference between the intensities from the two. The reduced PL intensity at the meeting fronts may be partly due to a probe-size-related artifact as a weak drop has also been observed in the near-field reflection intensity (reflection of 325 nm laser light) at the meeting fronts. The larger size of the NSOM probe (350 nm aperture size) compared to conventional AFM tips may result in the partial blockage of the luminescence or the reduction of the excitation density when it experiences abrupt height changes related to surface features. The increased PL intensity in the wing regions of the ELO samples compared to the window regions suggests improvement of the material quality in the wings by reduction of dislocations (also verified by TEM measurements discussed earlier) that act as and/or cause nonradiative recombination channels. Similar to sample B, sample C (20 μm stripe sample) also showed a weaker average PL intensity in the window regions and at the meeting fronts compared to the wing regions [see Figs. 8(c) and 8(d)]. However, the N-polar wings in sample C as compared to the Ga-polar wings demonstrate a weaker PL intensity, suggesting inferior optical quality of the N-polar wings. Additionally, the average PL intensity from the Ga-polar wings in sample C is less than one sixth of that in sample B. These results indicate that the material quality is certainly inferior for sample C, which also exhibited a larger (11$\bar{2}$0) reflection FWHM value of 0.27° for ϕ=0°.

Low temperature PL spectra were measured for sample B using 325 nm excitation from a HeCd laser, as shown in Fig. 9. The near band edge emission at 15 K is composed of two peaks at 3.475 and 3.419 eV [see Fig. 9(a)]. The 3.475 eV peak, which has a FWHM value of 19 meV, is a combination of the free exciton and donor bound exciton transitions, which are broad and cannot be delineated even at 15 K. As shown in Fig. 9(b), this main peak slightly blueshifts with increasing temperature up to 50 K and then starts to
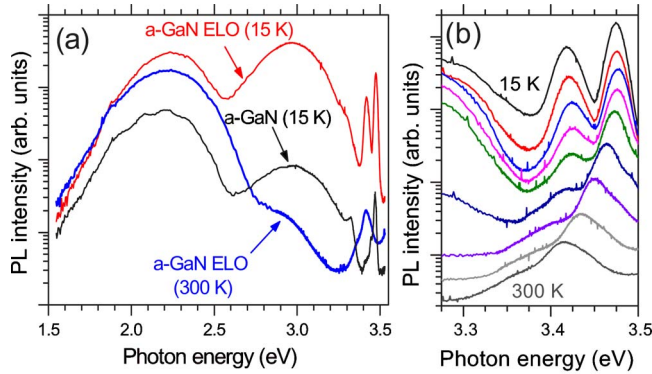
FIG. 9. (Color online) (a) PL spectra for sample B at 15 and 300 K and for the control *a*-plane GaN sample at 15 K. (b) PL spectra for sample B at temperatures 15, 25, 50, 75, 100, 150, 200, 250, and 300 K (from top to bottom and vertically shifted for clarity).

redshift reaching 3.415 eV at 300 K. This blueshift up to 50 K is due to the dissociation of the bound exciton with increasing thermal energy, which makes the free exciton peak dominant. The peak at 3.419 eV for the 15 K PL is most probably due to recombination of carriers/excitons bound to stacking faults[22] and also to other structural defects on the surface.[23] The band edge emission from sample B is approximately two orders of magnitude stronger than that from an *a*-plane GaN template on *r*-plane sapphire without ELO under identical measurement conditions [see Fig. 9(a)]. The characteristic blue and yellow emission bands are also observed with peaks around 2.96 and 2.25 eV, respectively. As shown in Fig. 9(a), the blue band and the band edge luminescence weaken significantly at 300 K while the intensity of the yellow band remains nearly unchanged.

TRPL measurements were also performed for sample B at room temperature. Figure 10 shows the 200 μJ/cm^2 excitation, band edge TRPL data (normalized to one) for the *a*-plane GaN ELO sample B and also for a standard *a*-plane GaN template. The decays for all the samples can be well characterized by a biexponential decay function

$A_1 \exp(-t/\tau_1) + A_2 \exp(-t/\tau_2)$. The fitting parameters for sample B are $\tau_1 = 0.08$ ns, $\tau_2 = 0.25$ ns, and $A_2/A_1 = 1.63$ at the band edge emission peak energy. Both of the measured decay times, τ_1 (short) and τ_2 (long), are limited by nonradiative recombination, and longer decay times and larger A_2/A_1 ratios indicate reduced nonradiative relaxation pathways. The inset of Fig. 10 shows the room temperature near band edge PL spectrum along with the effective PL decay times $\tau_{\mathrm{eff}} = (A_1\tau_1 + A_2\tau_2)/(A_1 + A_2)$ measured at different photon energies. The representative τ_{eff} near the band edge is approximately 0.2 ns. The radiative (τ_R) and nonradiative (τ_{NR}) lifetimes can be roughly estimated from the effective PL decay times using $1/\tau_{\mathrm{eff}} = 1/\tau_R + 1/\tau_{\mathrm{NR}}$ and substituting the equivalent internal quantum efficiency $\eta = 1/(1 + \tau_R/\tau_{\mathrm{NR}})$ with the spectrally integrated PL intensity at room temperature normalized to that at 10 K ($\eta = 0.032$ at room temperature). The resulting τ_R and τ_{NR} values are 6.45 and 0.21 ns, respectively. The decay times for the *a*-plane ELO sample are significantly longer compared to the standard *a*-plane GaN template (see Fig. 10), for which the system response ($\sim$40 ps) was not fast enough to resolve the exact PL decay. The improvement in decay times with *a*-plane ELO suggests reduction of nonradiative channels caused by the structural defects and the associated point defects, consistent with the TEM and NSOM observations discussed earlier.

IV. CONCLUSIONS

By employing a two-stage ELO of *a*-plane GaN with an initially enhanced vertical growth followed by enhanced lateral growth at an elevated temperature, Ga- to N-polar wing width ratio, and therefore, the wing height difference at the coalescence fronts have been reduced, resulting in a relatively flat, fully coalesced surface. TEM studies indicated the formation of new boundaries on inclined prismatic planes and dislocations along the vertical growth direction at the coalescence fronts due to the formation of a step between the two wings. In spite of this, the threading dislocation density was reduced from 4.2×10^{10} cm^{-2} in the window regions to 1.0×10^8 cm^{-2} in the wing regions, which still had a relatively high basal stacking fault density of 1.2×10^4 cm^{-1}. The improvement in the overgrown layer quality by ELO was also verified by NSOM and TRPL measurements, with the former showing strongly enhanced luminescence from the wing regions, while the latter indicated longer decay times compared to a standard *a*-plane GaN template.
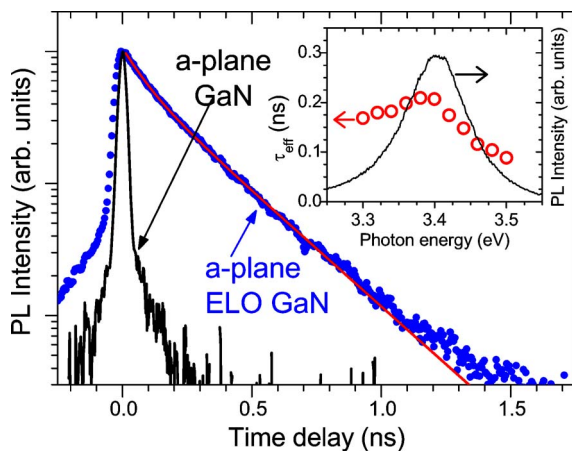
FIG. 10. (Color online) Normalized room temperature time-resolved PL for sample B and a standard *a*-plane GaN template. Solid line represents the biexponential fit to data. The inset shows the near band edge PL at room temperature and the effective PL decay times (τ_{eff}) at different photon energies.

[1]H. Morkoç, *Nitride Semiconductors and Devices* (Springer, Berlin, 1999), Chap. 2, p. 8.
[2]R. Langer, J. Simon, V. Ortiz, N. T. Pelekanos, A. Barski, R. Andre, and

M. Godlewski, Appl. Phys. Lett. **74**, 3827 (1999).

[3]T. Deguchi, K. Sekiguchi, A. Nakamura, T. Sota, R. Matsuo, S. Chichibu, and S. Nakamura, Jpn. J. Appl. Phys., Part 2 **38**, L914 (1999).

[4]H. M. Ng, Appl. Phys. Lett. **80**, 4369 (2002).

[5]M. D. Craven, S. H. Lim, F. Wu, J. S. Speck, and S. P. DenBaars, Appl. Phys. Lett. **81**, 469 (2002).

[6]X. Ni, Y. Fu, Y. T. Moon, N. Biyikli, and H. Morkoç, J. Cryst. Growth **290**, 166 (2006).

[7]H. M. Ng, A. Bell, F. A. Ponce, and S. N. G. Chu, Appl. Phys. Lett. **83**, 653 (2003).

[8]T. Koida, S. F. Chichibu, T. Sota, M. D. Craven, B. A. Haskell, J. S. Speck, S. P. DenBaars, and S. Nakamura, Appl. Phys. Lett. **84**, 3768 (2004).

[9]A. Chitnis, C. Chen, V. Adivarahan, M. Shatalov, E. Kuokstis, V. Mandavilli, J. Yang, and M. A. Khan, Appl. Phys. Lett. **84**, 3663 (2004).

[10]A. Sakai, H. Sunakawa, and A. Usui, Appl. Phys. Lett. **73**, 481 (1998).

[11]M. D. Craven, S. H. Lim, F. Wu, J. S. Speck, and S. P. DenBaars, Appl. Phys. Lett. **81**, 1201 (2002).

[12]C. Chen, J. Yang, H. Wang, J. Zhang, V. Adivarahan, M. Gaevski, E. Kuokstis, Z. Gong, M. Su, and M. A. Khan, Jpn. J. Appl. Phys., Part 2 **42**, L640 (2003).

[13]P. Fini, H. Marchand, J. P. Ibbetson, S. P. DenBaars, U. K. Mishra, and J. S. Speck, J. Cryst. Growth **209**, 581 (2000).

[14]Z. Liliental-Weber, D. Zakharov, B. Wagner, and R. F. Davis, Proc. SPIE **6121**, 612101 (2006).

[15]D. Hull and D. J. Bacon, *Introduction to Dislocation* (Pergamon, Oxford, 1984), Chap. 6, p. 112.

[16]Z. Liliental-Weber, M. Benamara, W. Swider, J. Washburn, J. Park, P. A. Grudowski, C. J. Eiting, and R. D. Dupuis, MRS Internet J. Nitride Semicond. Res. **4S1**, G4.6 (2000).

[17]X. Ni, Ü. Özgür, A. A. Baski, H. Morkoç, L. Zhou, D. J. Smith, and C. A. Tran, Appl. Phys. Lett. **90**, 182109 (2007).

[18]M. Syväjärvi, R. Yakimova, and E. Janzén, J. Cryst. Growth **208**, 409 (2000).

[19]J. L. Weyher, S. Lazar, J. Borysiuk, and J. Pernot, Phys. Status Solidi A **202**, 578 (2005).

[20]D. Zhuang and J. H. Edgar, Mater. Sci. Eng., R. **48**, 1 (2005).

[21]Z. Bougrioua, M. Laügt, P. Vennéguès, I. Cestier, T. Gühne, and E. Frayssinet, Phys. Status Solidi A **204**, 282 (2007).

[22]P. P. Paskov, R. Schifano, T. Paskova, T. Malinauskas, J. P. Bergman, B. Monemar, S. Figge, and D. Hommel, Physica B (Amsterdam) **376–377**, 473 (2006).

[23]M. A. Reshchikov and H. Morkoç, J. Appl. Phys. **97**, 061301 (2005).